JOURNAL OF SYNCHROTRON RADIATION
ISSN 1600-5775

Versatile variable temperature insert at the DEIMOS beamline for *in situ* electrical transport measurements

L. Joly,[a]* B. Muller,[a] E. Sternitzky,[a] J.-G. Faullumel,[a] A. Boulard,[a] E. Otero,[b] F. Choueikani,[b] J.-P. Kappler,[b] M. Studniarek,[a,b] M. Bowen[a] and P. Ohresser[b]

[a]Institut de Physique et de Chimie des Materiaux de Strasbourg, Université de Strasbourg, UMR 7504, 23 Rue du Loess, BP 43, 67034 Strasbourg Cedex 2, France, and [b]Synchrotron SOLEIL, L'Orme des Merisiers, Saint-Aubin, BP 48, 91192 Gif-sur-Yvette, France. *Correspondence e-mail: loic.joly@ipcms.unistra.fr

Received 4 December 2015
Accepted 11 February 2016

Edited by S. Svensson, Uppsala University, Sweden

Keywords: cryogenic insert; X-ray absorption spectroscopy; magnetic and electrical orders; multiferroics.

The design and the first experiments are described of a versatile cryogenic insert used for its electrical transport capabilities. The insert is designed for the cryomagnet installed on the DEIMOS beamline at the SOLEIL synchrotron dedicated to magnetic characterizations through X-ray absorption spectroscopy (XAS) measurements. This development was spurred by the multifunctional properties of novel materials such as multiferroics, in which, for example, the magnetic and electrical orders are intertwined and may be probed using XAS. The insert thus enables XAS to *in situ* probe this interplay. The implementation of redundant wiring and careful shielding also enables studies on operating electronic devices. Measurements on magnetic tunnel junctions illustrate the potential of the equipment toward XAS studies of *in operando* electronic devices.

1. Introduction

The soft X-ray beamline Dichroism Experimental Installation for Magneto-Optical Spectroscopy (DEIMOS) at the French synchrotron SOLEIL (Ohresser *et al.*, 2013, 2014; Joly *et al.*, 2014) is dedicated to the study of the electronic and magnetic properties of matter using polarized light. The DEIMOS beamline is fully optimized for the measurement of X-ray absorption spectroscopy (XAS) and X-ray magnetic dichroism (XMCD), which probe electronic and magnetic properties with chemical and orbital selectivity. The photon beam is optimized to obtain a high stability in energy and beam positioning so as to achieve highly reproducible measurements (Ohresser *et al.*, 2014) on very small amounts of material (Ohresser *et al.*, 2005; Mannini *et al.*, 2010; Tancini *et al.*, 2013; Corradini *et al.*, 2014; Giovanelli *et al.*, 2014), either at surfaces or species embedded in bulk samples.

The XAS measurement is obtained *via* the total fluorescence yield (TFY), or the total electron yield (TEY) techniques as a function of the photon energy (see for instance Stöhr, 1992). XMCD is performed by varying both the direction of an applied magnetic field and the helicity of the incoming X-ray photons. In some cases, it is possible to extract the magnetic orbital and spin moment of the probed sample through the so-called sum rules (Thole *et al.*, 1992; Carra *et al.*, 1993; Chen *et al.*, 1995).

The existing cryogenic insert enables measurements of absorption spectra under magnetic field in the temperature range 1.5–370 K, but without electrical wiring. The versatile

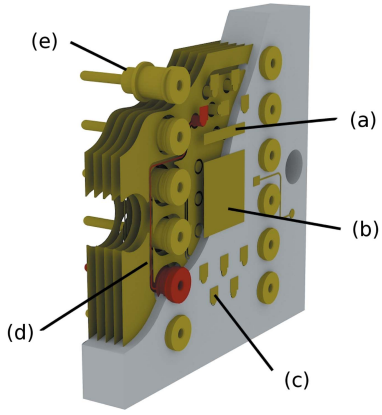

variable temperature insert (V^2TI) presented in this paper was designed to increase the sample environment capabilities of the DEIMOS beamline by adding electrical wiring in order to electrically polarize the sample, measure electrical voltages or currents, to operate a device (*e.g.* a piezo-electric motor) or any applications that require electrical wiring.

This ability could foster progress regarding research both in material and in physical science. For example, multiferroic materials exhibit simultaneously several ferroic orders. The most studied ones include ferroelectric and magnetic ordering, which suggests new device applications (Cheong & Mostovoy, 2007; Ramesh & Spaldin, 2007). XAS is a powerful technique to probe the electronic structure of this class of materials, especially when augmented by the electrical functionality proposed by the V^2TI insert. Another example, the transport phenomenon of solid-state tunnelling, as implemented in magnetic tunnel junctions (MTJs) (Miao *et al.*, 2011) within the research domain of spintronics (Chappert *et al.*, 2007), is understood to preserve both the spin and symmetry of the electron wavefunction. Yet the tunnelling magnetoresistance ratio (TMR), which expresses the degree to which these transmission channels are conserved, subsumes many elements such as the structural/chemical properties of the interface (Telesca *et al.*, 2012) or the presence of structural defects such as oxygen vacancies in the tunnel barrier of 'simple' MgO (Schleicher *et al.*, 2014). If XAS could be used on a working device, then a better understanding of how these microstructural aspects craft the device state (*e.g.* the TMR ratio) would be achieved. Yet, the ability to achieve a multi-state MTJ with either paraelectric $SrTiO_3$ with altered stoichiometry (Bowen *et al.*, 2006*a*), or nominally ferroelectric $BaTiO_3$ (Garcia *et al.*, 2010), underscores the need to precisely pinpoint the origin of the electrical functionality of the device. XAS studies on an operating device are clearly relevant here.

2. Specifications/needs

The V^2TI should enable low-energy XAS and XMCD measurements at low temperature on an electrically contacted sample. As the experiment is located at a synchrotron facility, the operation of the V^2TI and its capabilities must be as user efficient and accessible as possible. We emphasize here that many of the numerous users may not necessarily have any prior training on this particular equipment, or even on a transport experiment in general. These considerations therefore require careful design of the V^2TI, notably to enable fast sample switching so as to minimize measurement downtime.

The full range of investigated samples is very broad. This implies that the sample temperature range has to be large, from room temperature for devices aiming to be industrially produced, to low temperature for fundamental studies (below 20 K). As devices may be electrostatically sensitive, we have to ensure that a reasonable number of devices remain intact during the several steps between device fabrication and exposure to the measurement conditions [room or low temperature, under the X-ray beam within ultra-high vacuum (UHV) conditions] while they are electrically connected. So increasing the experimental success rate requires the ability to probe as many devices as possible.

These specifications can be summarized as follows:

(i) Simple and fast sample transfer in UHV conditions.

(ii) Device temperature below 20 K.

(iii) Differing geometries of X-ray incidence onto the sample. We chose two orientations (0° and 45°) relative to the incoming X-ray beam.

(iv) Twelve wires connected to the sample(s) for users' requirements.

(v) Ability to easily electrically connect user devices using wire-bonding.

(vi) Electrically insulated sample to enable TEY measurements.

The challenge here is to achieve 12 wire connections on a sample holder that is electrically insulated toward TEY studies, yet thermally conductive so as to achieve low device temperatures. This challenge is compounded by the various electrical connections that are established, from the UHV flange to the user-removable sample and its devices. Notably, this implies a device environment that is both UHV and microelectronics compatible.

3. The V^2TI design

In this section, we describe the design of the new V^2TI head and the sample holder. This horizontal insert can be installed into either of the CroMag or 2 Tesla electro-magnet (MagneTwo) endstations available at the DEIMOS beamline (Ohresser *et al.*, 2014). As the CroMag sample environment is better suited for devices that require cryogenic conditions, all the measurements tests were performed using this endstation.

This insert is based on an UHV cryostat produced by Janis (reference ST-402) that operates within 1.8 K to 420 K. At the extremity of the commercial cold finger, we mount our homemade head (Fig. 1, top left). This head consists of a sample holder interface that extends the cold finger so as to provide 16 electrical connections. To ensure both a very good electrical insulation (the resistance between sample and ground has to be larger than 200 GΩ) and a good thermal conductivity between the Janis cryostat (Fig. 1*d*) and the sample interface (Fig. 1*a*), we used a sapphire disc (Fig. 1*b*) sandwiched between two copper parts (Figs. 1*a* and 1*c*). The electrical contacts from outside to the sample are achieved on account of the specific design and the use of three different printed circuit boards (PCBs). We describe these successive connections in more detail hereafter. On the sample interface (Fig. 1*a*) the connections are arranged in a circle around a threaded hole. The sample holder can then be screwed into this thread following the standard sample holder transfer procedure used on the DEIMOS beamline and while achieving both the electrical contacts and thermal conductivity required for the measurements. These electrical connections are then extended to a sample chip that can be plugged into the sample holder (Fig. 1, top right). Note that only 12 electrical connections will be used at the same time because of limited free space on the sample chip.

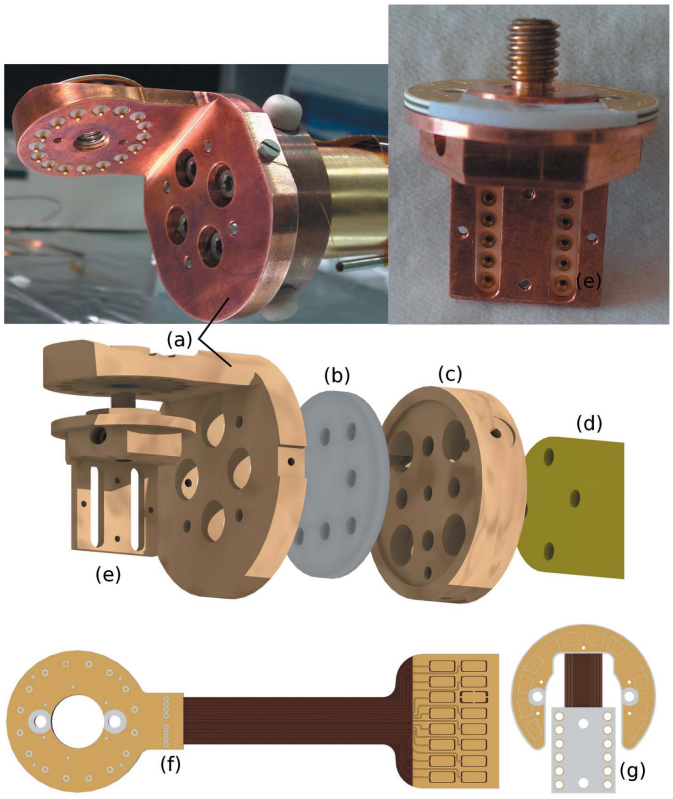

Figure 1
Immediate sample environment. Top: photographs of the insert (left) and the sample holder (right). The middle view is an expanded view of the homemade head where the main parts are without screws or PCB: (*a*) sample holder interface; (*b*) sapphire disc; (*c*) interface between the Janis cryostat and the sapphire disc; (*d*) the commercial cryostat from Janis; (*e*) the sample holder. Bottom: flat view of (*f*) the top PCB with Kapton flex and (*g*) the sample holder PCB.

3.1. Electrical insulation

In order to detect the TEY current, the sample has to be insulated from all other signals. The 16 signal wires that flow through the PCBs are insulated from the TEY by the PCB insulating material itself, which consists of a hydrocarbon/ceramic compound (reference Roger RO4000 series, UHV compatible, bakeable). This material is a proprietary woven-glass-reinforced hydrocarbon/ceramic laminate designed for performance-sensitive applications, with a temperature-independent dielectric constant, a good thermal conductivity at low temperature, an electrical resistivity of $1.7 \times 10^{16}\ \Omega$ cm at room temperature and a coefficient of thermal expansion similar to that of copper. The low dielectric tolerance and low loss provide us with excellent electrical performance.

The three specific PCBs (Figs. 1*f*, 1*g* and 3) are stacks of copper tracks and hydrocarbon/ceramic insulation layers. The internal copper tracks of the PCB have a 35 µm-thick layer of copper and 300 µm of insulation.

The TEY current passes through the PCB of the sample chip to the PCB of the sample holder, which is itself in contact with the sample holder interface.

3.2. The sample holder

The sample holder (Fig. 1*e*) is machined with high purity copper and equipped with a copper–beryllium screw. Starting from the sample, 12 electrical connections (Fig. 2*a*) flow through the sample PCB chip (Fig. 2*b*), the sample holder PCB (Fig. 1*g*), and the Kapton flexible part (Fig. 2*f*) to the sample holder PCB electrical contacts (Fig. 2*c*). The sample holder PCB, the sample PCB chip (Fig. 2*b*) and the Teflon part (Fig. 2*d*) are held in place using molybdenum screws.

In order to characterize the properties of a sample, the sample chip is clipped onto the sample holder (in air) prior to UHV transfer. To guarantee a good thermal contact the sample holder is screwed at room temperature onto the cold finger.

As user samples may be microelectronics-based and electrostatically sensitive, the sample chip is provided ahead of the beam time so that users can connect their devices to the sample chip in a previously vetted manner (*e.g.* in their laboratory). This also enables verification of the electrical connections and device operation prior to UHV insertion, so as to optimize beam time efficiency. Ideally, the beam time begins with the users simply mounting their previously prepared sample chip onto a sample holder and inserting into the load-lock.

The sample chip itself is also a multilayer PCB (see Fig. 3) made of the same material as the aforementioned PCBs. The chip was designed to optimize the thermal conductivity to the

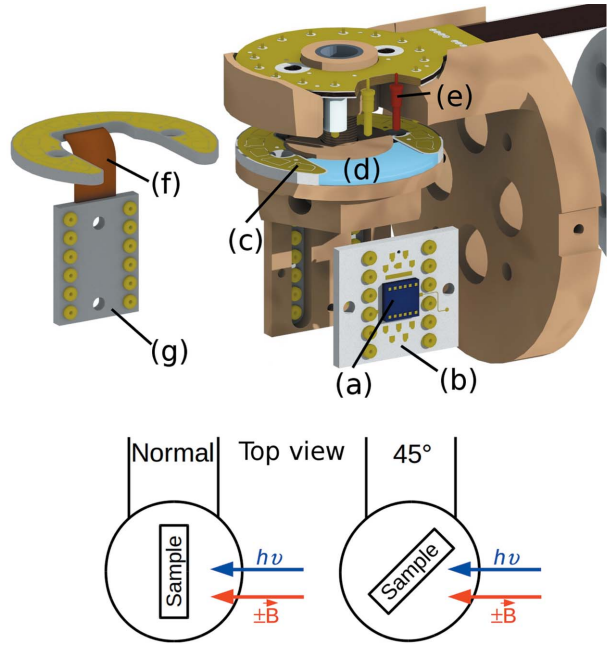

Figure 2
The top view shows the unscrewed sample holder, without the screws for clarity and semi-transparent to see the spring dots: (*a*) sample (dark blue), (*b*) sample PCB chip ready to be plugged into (*g*), (*c*) 12 electrical contacts, (*d*) Teflon part, (*e*) spring dot, (*f*) Kapton flex, (*g*) sample holder PCB. The bottom view is a top-view sketch showing the direction of photons $h\upsilon$ and the direction of the magnetic field $\pm\mathbf{B}$ for the normal and the 45° angle of incidence.

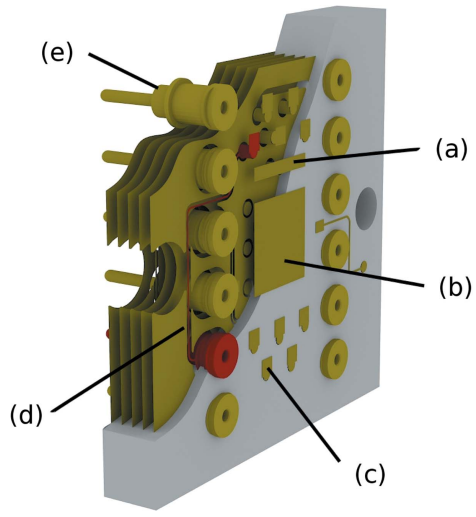

Figure 3
The multiple layers of the sample chip (yellow is copper, white is insulator): (*a*) TEY pad; (*b*) sample pad; (*c*) bonding pad; (*d*) internal copper track connecting a tulip pin and a bonding pad; (*e*) tulip pin.

user sample by introducing bridges (with 12 vias) between the lowest track (in contact with the sample holder) and the track just below the top track sample pad. Note that the sample pad (Fig. 3*b*) is not electrically connected to the TEY wire so that the user may choose whether to measure the TEY signal or not (rectangular pad, Fig. 3*a*).

Finally, the top of the sample chip provides 12 gold bonding pads (Fig. 3*c*) for microbonding or gluing that are electrically connected to the sample chip tulips (Fig. 3*e*).

3.3. Tests measurements

The TEY current is measured using an insulated wire connected to the sample holder interface (Fig. 1*a*). This dedicated TEY wire is separated from the other wires and is connected to a separate BNC outside connector through a flange mounted at the top of the Janis cryostat.

The leakage current (obtained from the TEY connection to the ground) without any device mounted on a sample chip is about 50 ± 10 fA. When an electrical current of about 20 µA flows through a device (similar to the MTJs described in §4), the TEY leakage current is about 70 ± 10 fA, which is independent of the device and thus the connection used. This leakage current is very low with respect to the pA–nA range TEY current. This implies that a TEY measurement will be possible during the injection of an electrical current into a sample.

In addition to the TEY measurement, the TFY can be obtained by means of a photodiode installed on the 77 K shield of the cryomagnet at 90° with respect to the beam direction. The presence of this photodiode is mandatory in the case of an insulating sample, for instance.

To measure the sample temperature a temperature sensor (reference Scientific Instrument Si410C, excitation current: 10 µA) was positioned at the precise position of the sample [Fig. 2(*a*), over the square gold pad Fig. 3(*b*)]. With the exchanger of the Janis cryostat at 4.2 K, we reached a temperature of 12 K at the sample, for a liquid He consumption of about 0.6 L h^{-1}.

4. Testing a micro-electronics device

MgO-based MTJs currently represent an essential cornerstone of spintronics, with inroads into spin-torque nano-oscillators, MRAM and magnetic sensors. The large spintronic response (TMR) of these MTJs essentially underscores the dominant transmission of charge carriers with Δ1 (Δ5) electronic symmetry in the parallel (antiparallel) orientation of electrode magnetization (denoted P and AP) (Butler *et al.*, 2001). This dominant transmission reflects (i) spin- and symmetry-dependent wavefunction hybridization at the junction interfaces, which notably leads to magnetic moments on the barrier of the interfacial atoms (Bowen *et al.*, 2006*b*; Valencia *et al.*, 2011; Djeghloul *et al.*, 2013) and (ii) the symmetry-dependent exponential decay parameter from complex band structure considerations (Butler *et al.*, 2001; Bowen *et al.*, 2006*c*). A mixing of symmetry channels may occur when solid-state tunnelling is mediated by structural defects in the tunnel barrier (Schleicher *et al.*, 2014).

The MTJs are fabricated at the Institut de Physique et Chimie des Matériaux de Strasbourg (IPCMS) with clean-room techniques (Halley *et al.*, 2008) using the following stack grown at the Institut Jean Lamour (IJL), Nancy (Bernos *et al.*, 2010): glass / Ta (5 nm) / Co (10 nm) / IrMn (7.5 nm) / FeCoB (4 nm) / MgO (2.5 nm) / FeCoB (5 nm) / Ta (5 nm) / Pt (3 nm). The MTJs are then tested and five (resp. 10) are chosen for four-point measurements (resp. two-point measurements) and then bonded on the DEIMOS chip to the bonding pads (Fig. 4*b*), to be finally transported to Synchotron SOLEIL. These MTJs exhibit a TMR ratio of about 100% at T = 300 K.

The overarching difficulty is to obtain working devices under the X-ray beam after device preparation/testing at the IPCMS, installation into the loadlock, transfer through several chambers and mounting on the Cu cold finger extension.

An important result of the first studies is that it is possible, given enough attempts, to measure MTJs at beamline DEIMOS despite their electrostatic fragility. This highlights why, when testing electrostatically sensitive devices, a large number of electrical contacts to the sample is crucial. Of the 37 bonded and tested MTJs, only 20% were still working when mounted on the V^2TI insert, compared with a 90% success rate at the IPCMS laboratory.

We present in Fig. 4(*a*) a low-resolution map of X-ray absorption at the Co L_3-edge (788 eV), performed in fluorescence mode (X-ray beam impinging at 45° onto the sample), of a representative sample containing MTJs. We acquired this map by using the motors of the Cromag cryomagnet support to move the sample relative to the X-ray beam position. Here the size of the beam was 110 µm (H) × 80 µm (V) (Ohresser *et al.*, 2014). Comparing with the visible light picture of Fig. 4(*b*), one clearly distinguishes DEIMOS chip features such as tulip pins and the overall features of a lower electrode containing 12 MTJs. A high-resolution (20 µm steps) scan then allowed us

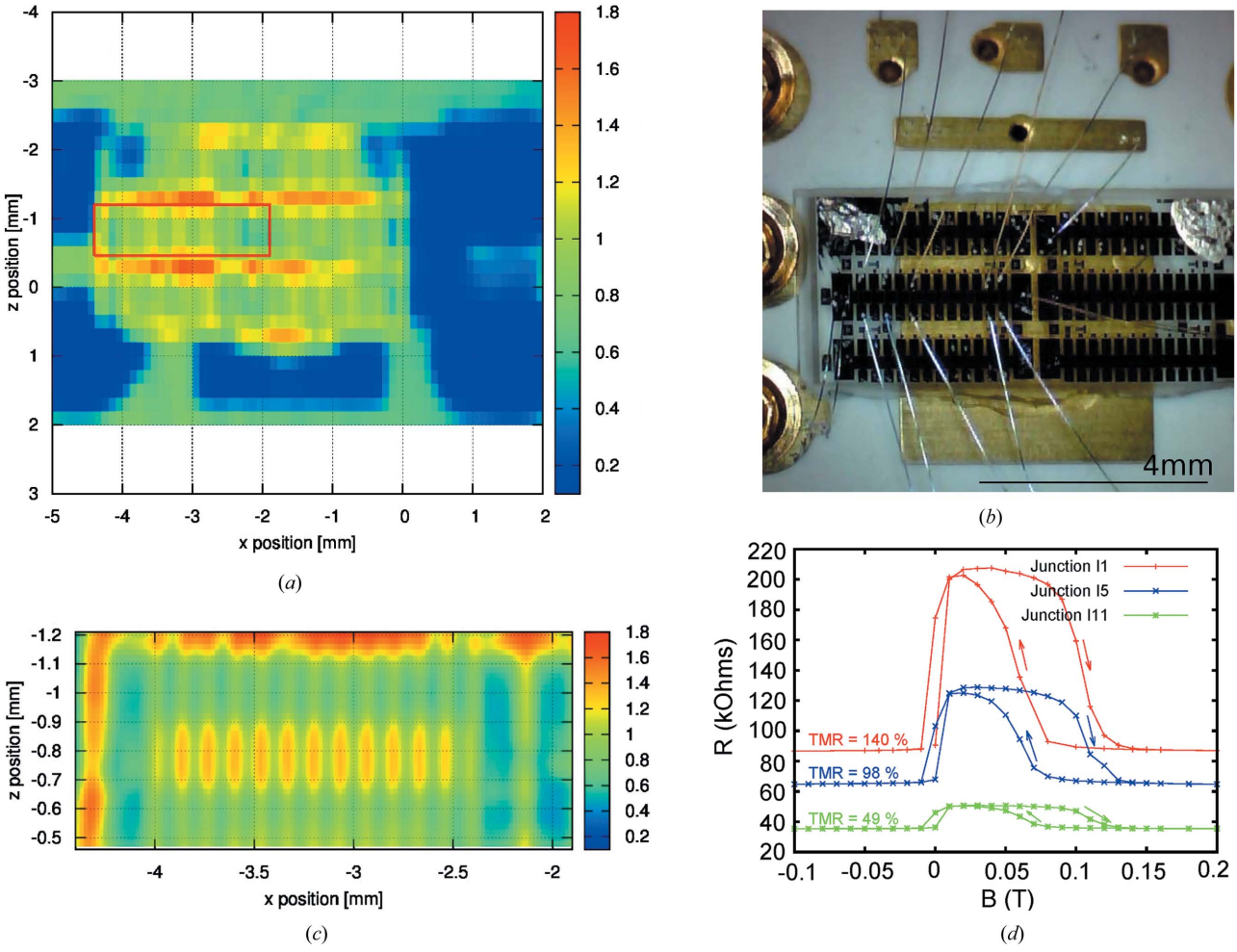

Figure 4
Magnetic tunnel junctions at beamline DEIMOS. (*a*) Coarse sample scan at 788 eV (Co L_3-edge) of the sample. The region of electrical interest is outlined in red. (*b*) Visible light picture of a sample containing 77 MTJs mounted on a DEIMOS chip, with five MTJs bonded in four-point mode *via* the 12 pins. (*c*) High-resolution scan (20 µm steps) of the probed MTJs. The low signal corresponds to metal contacts on both the lower and the top electrodes, whereas the red portions correspond to probing the lower electrode between the top electrode contacts. (*d*) Magnetotransport measurements at DEIMOS beamline. Resistance as a function of the magnetic field $R(H)$ with an applied voltage of 5 mV at room temperature for three different MTJs. No X-rays were applied.

to pinpoint each MTJ within a given common lower electrode (see Fig. 4*c*). The spatial coordinates for motor positioning then allowed us to optically target a precise MTJ with the X-ray beams.

We present in Fig. 4(*d*) a set of $R(H)$ curves [resistance (R) of the sample as a function of the magnetic field (H)] measured at T = 300 K and with a sample bias of V = 5 mV that shows TMR values for several devices ranging from 49% to 140%, as expected. These data were acquired by separately recording $R(t)$ and $H(t)$. Future improvements to the V^{2}TI user environment shall include the ability to transparently request a fully automated $R(H)$ measurement. Results on MTJs exposed to X-ray radiation will be presented elsewhere.

5. Conclusions

X-ray absorption spectroscopy provides a sensitive chemical probe of the electronic properties of a material. As, for many materials, these properties may be modified through electrical stimuli, and with the aim to better pinpoint how the electrical stimulus alters these properties, beamline DEIMOS at Synchrotron SOLEIL has equipped itself with an electrical insert to achieve this capability. In this paper, we presented a detailed description of the design and the performances of this V^{2}TI insert.

Particular care was given to achieve a device environment compatible with micro-electronics. The presented results demonstrate that it is possible to study electrostatically sensitive devices at the DEIMOS beamline. To the best of our knowledge, these are the first magneto-transport measurements of a magnetic tunnel junction within a synchrotron-grade experiment. This opens interesting opportunities to probe, using synchrotron radiation, the properties of a working electronic device.

Future developments will focus on synchronizing and automating electrical stimuli within the parameter space of

beamline DEIMOS, notably, with the aim to demonstrate measurement reproducibility. One goal is to achieve concurrent electrical and optical multiplexing with visible light on devices developed at the IPCMS laboratory (Halisdemir *et al.*, 2016).

Acknowledgements

This work has been supported by the Region Ile-de-France in the framework of DIM nanoK 'des atomes froids aux nanosciences'. We are grateful to the SOLEIL staff for smoothly running the facility. We thank M. Hehn of IJL, Nancy, for providing MTJ stacks. We acknowledge the STNano technological platform for access and its staff for help. MTJ testing within this work was made possible through grants from the ANR (ANR-09-JCJC-0137, ANR-14-CE26-0009-01), Labex NIE ANR-11-LABX-0058_NIE 'Symmix', the CNRS (STII PEPS 'SpinTrans', PICS 'Oxyspin'), the University of Strasbourg and La Région Alsace.

References

Bernos, J., Hehn, M., Montaigne, F., Tiusan, C., Lacour, D., Alnot, M., Negulescu, B., Lengaigne, G., Snoeck, E. & Aliev, F. G. (2010). *Phys. Rev. B*, **82**, 060405.

Bowen, M., Barthélémy, A., Bellini, V., Bibes, M., Seneor, P., Jacquet, E., Contour, J.-P. & Dederichs, P. H. (2006*c*). *Phys. Rev. B*, **73**, 140408.

Bowen, M., Cros, V., Jaffrès, H., Bencok, P., Petroff, F. & Brookes, N. B. (2006*b*). *Phys. Rev. B*, **73**, 012405.

Bowen, M., Maurice, J. L., Barthélémy, A., Prod'homme, P., Jacquet, E., Contour, J. P., Imhoff, D. & Colliex, C. (2006*a*). *Appl. Phys. Lett.* **89**, 103517.

Butler, W. H., Zhang, X.-G., Schulthess, T. C. & MacLaren, J. M. (2001). *Phys. Rev. B*, **63**, 054416.

Carra, P., Thole, B. T., Altarelli, M. & Wang, X. (1993). *Phys. Rev. Lett.* **70**, 694–697.

Chappert, C., Fert, A. & Van Dau, F. N. (2007). *Nat. Mater.* **6**, 813–823.

Chen, C. T., Idzerda, Y. U., Lin, H.-J., Smith, N. V., Meigs, G., Chaban, E., Ho, G. H., Pellegrin, E. & Sette, F. (1995). *Phys. Rev. Lett.* **75**, 152–155.

Cheong, S.-W. & Mostovoy, M. (2007). *Nat. Mater.* **6**, 13–20.

Corradini, V., Ghirri, A., Candini, A., Biagi, R., del Pennino, U., De Renzi, V., Dotti, G., Otero, E., Hooper, T. N., Inglis, R., Brechin, E. K. & Affronte, M. (2014). *Adv. Funct. Mater.* **24**, 4782–4788.

Djeghloul, F. *et al.* (2013). *Sci. Rep.* **3**, 1272.

Garcia, V., Bibes, M., Bocher, L., Valencia, S., Kronast, F., Crassous, A., Moya, X., Enouz-Vedrenne, S., Gloter, A., Imhoff, D., Deranlot, C., Mathur, N. D., Fusil, S., Bouzehouane, K. & Barthélémy, A. (2010). *Science*, **327**, 1106–1110.

Giovanelli, L., Savoyant, A., Abel, M., Maccherozzi, F., Ksari, Y., Koudia, M., Hayn, R., Choueikani, F., Otero, E., Ohresser, P., Themlin, J. M., Dhesi, S. S. & Clair, S. (2014). *J. Phys. Chem. C*, **118**, 11738–11744.

Halisdemir, U. *et al.* (2016). Submitted.

Halley, D., Majjad, H., Bowen, M., Najjari, N., Henry, Y., Ulhaq-Bouillet, C., Weber, W., Bertoni, G., Verbeeck, J. & Van Tendeloo, G. (2008). *Appl. Phys. Lett.* **92**, 212115.

Joly, L., Otero, E., Choueikani, F., Marteau, F., Chapuis, L. & Ohresser, P. (2014). *J. Synchrotron Rad.* **21**, 502–506.

Mannini, M., Pineider, F., Danieli, C., Totti, F., Sorace, L., Sainctavit, Ph., Arrio, M.-A., Otero, E., Joly, L., Cezar, J. C., Cornia, A. & Sessoli, R. (2010). *Nature (London)*, **468**, 417–421.

Miao, G.-X., Münzenberg, M. & Moodera, J. S. (2011). *Rep. Prog. Phys.* **74**, 036501.

Ohresser, P., Bulou, H., Dhesi, S. S., Boeglin, C., Lazarovits, B., Gaudry, E., Chado, I., Faerber, J. & Scheurer, F. (2005). *Phys. Rev. Lett.* **95**, 195901

Ohresser, P., Otero, E., Choueikani, F., Chen, K., Stanescu, S., Deschamps, F., Moreno, T., Polack, F., Lagarde, B., Daguerre, J. P., Marteau, F., Scheurer, F., Joly, L., Kappler, J. P., Muller, B., Bunau, O. & Sainctavit, Ph. (2014). *Rev. Sci. Instrum.* **85**, 013106.

Ohresser, P., Otero, E., Choueikani, F., Stanescu, S., Deschamps, F., Ibis, L., Moreno, T., Polack, F., Lagarde, B., Marteau, F., Scheurer, F., Joly, L., Kappler, J.-P., Muller, B. & Sainctavit, Ph. (2013). *J. Phys. Conf. Ser.* **425**, 212007.

Ramesh, R. & Spaldin, N. A. (2007). *Nat. Mater.* **6**, 21–29.

Schleicher, F. *et al.* (2014). *Nat. Commun.* **5**, 4547.

Stöhr, J. (1992). *NEXAFS Spectroscopy, Springer Series on Surface Science*, Vol. 25. Berlin/Heidelberg: Springer-Verlag.

Tancini, E., Mannini, M., Sainctavit, P., Otero, E., Sessoli, R. & Cornia, A. (2013). *Chem. Eur. J.* **19**, 16902–16905.

Telesca, D., Sinkovic, B., Yang, S.-H. & Parkin, S. S. P. (2012). *J. Electron Spectrosc. Relat. Phenom.* **185**, 133–139.

Thole, B. T., Carra, P., Sette, F. & van der Laan, G. (1992). *Phys. Rev. Lett.* **68**, 1943–1946.

Valencia, S., Crassous, A., Bocher, L., Garcia, V., Moya, X., Cherifi, R. O., Deranlot, C., Bouzehouane, K., Fusil, S., Zobelli, A., Gloter, A., Mathur, N. D., Gaupp, A., Abrudan, R., Radu, F., Barthélémy, A. & Bibes, M. (2011). *Nat. Mater.* **10**, 753–758.